Nanoscale Resolution of Electric-field Induced Motion in Ionic Diblock Copolymer Thin Films

Jason W. Dugger[1,†], Wei Li[1,†], Mingtao Chen[2], Timothy E. Long[2], Rebecca J. L. Welbourn[3], Maximilian W.A. Skoda[3], James F. Browning[4,*], Rajeev Kumar[1,5,**], Bradley S. Lokitz[1,***]

[1]Center for Nanophase Materials Sciences, Oak Ridge National Laboratory, Oak Ridge, TN 37831

[2]Macromolecules Innovation Institute (MII), Department of Chemistry, Virginia Tech, Blacksburg, VA 24061

[3]ISIS, Science and Technology Facilities Council, Rutherford Appleton Laboratory, Didcot, OX11 0QX, U.K.

[4]Neutron Scattering Division, Oak Ridge National Laboratory, Oak Ridge, TN 37831

[5]Computational Sciences and Engineering Division, Oak Ridge National Laboratory, Oak Ridge, TN 37831

[†]*Authors contributed equally to this work.*

**Correspondence for neutron reflectometry should be addressed to J.F.B. (browningjf@ornl.gov)*

***Correspondence regarding theory and simulations should be addressed to R.K. (kumarr@ornl.gov)*

****Experimental correspondence should be addressed to B.S.L. (lokitzbs@ornl.gov)*

*This manuscript has been authored by UT-Battelle, LLC under Contract No. DE-AC05-00OR22725 with the U.S. Department of Energy. The United States Government retains and the publisher, by accepting the article for publication, acknowledges that the United States Government retains a non-exclusive, paid-up, irrevocable, world-wide license to publish or reproduce the published form of this manuscript, or allow others to do so, for United States Government purposes. The Department of Energy will provide public access to these results of federally sponsored research in accordance with the DOE Public Access Plan (*http://energy.gov/downloads/doe-public-access-plan*).*

ABSTRACT: Understanding the responses of ionic block copolymers to applied electric fields is crucial when targeting applications in areas such as energy storage, microelectronics, and transducers. This work shows that the identity of counterions in ionic diblock copolymers substantially affects their responses to electric fields, demonstrating the importance of ionic species for materials design. *In situ* neutron reflectometry measurements revealed that thin films containing imidazolium based cationic diblock copolymers, tetrafluoroborate counteranions led to film contraction under applied electric fields, while bromide counteranions drove expansion under similar field strengths. Coarse-grained molecular dynamics simulations were used to develop a fundamental understanding of these responses, uncovering a non-monotonic trend in thickness change as a function of field strength. This behavior was attributed to elastic responses of microphase separated diblock copolymer chains to variations in interfacial tension of polymer-polymer interfaces, arising from the redistribution of counteranions in the presence of electric fields.

KEYWORDS: *ionic block copolymer, neutron reflectometry, electric field, molecular dynamics, interfacial tension*

1. INTRODUCTION

Polymerized ionic liquid based block copolymers (PIL-BCPs) are promising materials for many electrical applications such as batteries, fuel cells, photovoltaics, and electroresponsive transducers.[1-4] Typically, PIL-BCPs consist of ionic blocks linked to non-ionic and non-polar blocks in order to enhance mechanical integrity.[1-4] Immiscibility

of ionic and non-ionic blocks has significant effects on the microphase separation in such copolymers,[5-6] allowing control over accessible morphologies through electrostatics.[2-3, 7-9] Despite many advances related to microphase separation in PIL-BCPs,[5-6, 9-11] their responses to applied electric fields remain poorly understood and hinders their rational design for specific applications, such as minimizing material deformation while preserving conductivity for energy storage systems or maximizing strain for enhanced actuation of transducers.

Complications in understanding responses of PIL-BCPs to applied electric fields result from multiple mechanisms that can affect their behavior. These mechanisms include alignment of chains along the applied electric field due to dielectric mismatch between blocks,[12-14] electric field induced shifts in disorder-order transition temperatures,[15-17] redistribution of counterions,[18-20] and charge generation in applied electric fields.[21-23] In particular, counterions in PIL-BCPs are expected to alter the threshold electric field strength required to exhibit electroresponsiveness in a significant manner.[18-20] For example, thin films of typical non-ionic diblock copolymers exhibit structural changes in response to applied electric fields ~ 10 V/μm at temperatures above the glass transition temperature of one of the blocks.[24] By contrast, PIL-BCPs can exhibit responses at much lower electric field strengths (~0.25 V/μm), as demonstrated in this work. Furthermore, electrical responses are expected even at temperatures below the glass transition of the blocks.[25] Such enhancement of electroresponsiveness of PIL-BCPs is justified by theoretical considerations and simulations,[18] which highlight the importance of counterion

redistribution in applied electric fields as well as the mobile nature of counterions even when segmental dynamics are restricted.

There have been a number of reports[5-9, 11, 26-27] highlighting the dramatic effects of counterions on microphase separation in PIL-BCPs. It has been shown that electrostatic effects can be characterized by changes in the effective copolymer segregation strength (the Flory-Huggins parameter, χ_{eff}), which becomes dependent on counterion size, concentration, binding strengths with monomers, as well as dielectric mismatch between blocks.[7-9, 11, 28] Furthermore, counterion transport becomes anisotropic in PIL-BCPs and the effects of morphology on transport have been studied.[10, 27] However, to the best of our knowledge, there are no studies of nanoscale structural responses of PIL-BCPs in thin film geometries, which are vital to developing an understanding of the underlying mechanism of their electromechanical responsiveness.

To bridge this gap in understanding, thin films of cationic diblock copolymers were studied using neutron reflectometry in the presence of external electric fields. Specifically, the focus was on understanding the effects of counteranion identity and contrasting behaviors were observed while examining changes in the total thickness of the films in electric fields. Coarse-grained molecular dynamics simulations were used to interpret the experimental findings for developing an understanding of the origin of these thickness changes.

2. EXPERIMENTAL SECTION

2.1 Polymer Synthesis and Characterization. The ionic AB diblock copolymers used in this study were composed of ionic A blocks (PIL) containing 1-butyl-3-(10'-hydroxyl)imidazolium groups paired with either BF_4 or Br counteranions (see Figure S1). B blocks were constituted of polystyrene to provide structural support for the system, while the A blocks imparted electroresponsiveness to these copolymers. The full synthesis details of the ionic-liquid monomers have been reported elsewhere,[29] briefly: 1-butyl imidazole reacted with 10-bromo-1-decanol, and the resulting charged precursor was further reacted with methacryloyl chloride to yield ionic-liquid monomer. The synthesis of diblock copolymers was achieved through reversible addition-fragmentation chain-transfer (RAFT) polymerization. PIL-BCP-Br was synthesized as follows: PIL-Br (9.60 g, 0.022 mol), 4-Cyano-4-[(dodecylsulfanylthiocarbonyl)sulfanyl]pentanoic acid (CDP, 60.15 mg, 0.15 mmol), 2,2'-Azobis(2-methylpropionitrile) (AIBN, 8.16 mg, 0.05 mmol), and anhydrous acetonitrile (22.35 mL) were charged into a 50 mL, one-neck, round-bottomed flask, and sparged with argon for 40 mins. The reaction mixture was heated to 65 °C for 21 hrs under vigorous stirring. The resulting yellow macroCTA was precipitated into ethyl acetate and washed with ethyl acetate three times. After drying under vacuum at room temperature, the PIL-Br macroCTA (4.15 g) was dissolved in anhydrous DMF (23.21 mL) with deuterated styrene (5.2 g, 0.046 mol) and AIBN (6.77 mg, 0.04 mmol). The solution was sparged with argon for 40 mins, and reacted at 65 °C for 48 hrs. The resulting diblock copolymers (PIL-BCP-Br) were precipitated into ethyl acetate and washed with ethyl acetate three times. The product was further dried in vacuum at 50 °C for 1 d and yielded a brown solid. All structures were confirmed by ^{1}H NMR spectroscopy. The diblock copolymers with BF_4 counteranions (PIL-BCP-BF_4) were synthesized through post-polymerization ion exchange of PIL-BCP-Br in DMF with a large excess of $LiBF_4$ salt for 24 hrs under vigorous stirring followed by three washes with DI water. All structures were confirmed by ^{1}H NMR and ^{19}F NMR spectroscopy, which did not indicate the presence of residual salts following ion exchange. The absolute molecular weight of the diblock was determined to be 60 kDa with a 1.09 polydispersity index through size exclusion chromatography (SEC) (DMF +

0.05 M LiBr as mobile phase with a dn/dc of 0.0977 mL/g). The ratio of PIL to dPS was determined using ^{13}C NMR by comparing the signal intensities arising from the imidazolium ring of PIL and the styrene ring from the dPS block, resulting in a 2.5:1 ratio (cf. Table S1). Thermal transitions were measured by a TA Q2000 differential scanning calorimeter (DSC) under N_2(g). Reported values (middle point) were from the second heating cycle of a heat/cool/heat procedure: (1) 10 °C/min ramp from 23 to 150 °C, isotherm at 150 °C for 30 min, (2) 100 °C/min quench cool to -80 °C, and (3) 10 °C/min ramp to 150 °C. DSC samples were prepared in T-zero pans and the T_gs were measured after drying under vacuum for 18 hrs.

2.2 Thin Film Preparation. Round silicon wafers (0.005 Ω·cm resistivity, 51 mm in diameter, and 5 mm thick) (University Wafer Inc.) were sonicated for 5 min in acetone, isopropanol, and methanol and then dried under Ar(g). The wafers were then submerged in a piranha solution (3:1 concentrated sulfuric acid / 30% hydrogen peroxide — *Caution: explosive in the presence of organics*) for 30 min. The wafers were rinsed in high-purity water (>18 MΩ·cm) and dried under Ar(g). The diblock copolymers were dissolved in dimethylformamide (Fisher Scientific) at 3 wt/v% and sonicated for up to 1 hr before spin-coating onto the clean silicon wafers (4500 rpm for 30 sec). Samples were covered and allowed to anneal at room-temperature in a fume hood for 18 hrs and then placed in a vacuum oven at 120 °C for an additional 24 hrs. Ellipsometry was conducted on samples prepared similarly to those studied in NR using a Woollam M-2000U variable angle spectroscopic ellipsometer over a wavelength range of 245-999 nm as a complementary technique to confirm the film thicknesses. Those findings (data not reported) were consistent with the values obtained through NR.

2.3 Neutron Reflectometry. Reflectometry experiments were carried out using the INTER reflectometer at the ISIS facility of Rutherford Appleton Laboratory (RAL) (U.K.) as well as on the Liquids Reflectometer at the Spallation Neutron Source (SNS) of Oak Ridge National Laboratory

(ORNL) (U.S.). Measurements at the INTER reflectometer obtained Q_z values from 0.004 – 0.28 Å^{-1} by using discrete θ values of 0.3°, 0.5°, and 2.0° and a wavelength band of 1.5 – 17 Å. Data collected at the Liquids Reflectometer comprised seven settings using discrete incident angles 0.6°, 1.2°, and 2.3° and wavelength bands centered at 15.1, 12.4, 9.7, 4.3, and 4.2 Å achieving a Q_z range of 0.008 – 0.2 Å^{-1}. The same sample environment chamber was used to apply electric fields to the samples at both the ISIS and SNS facilities. This custom chamber was designed at ORNL with the assistance of Nor-Cal, Inc., which fabricated the components. A detailed description of this chamber will be published elsewhere. Samples were loaded into the chamber and positioned between two aluminum plates where the conductive silicon substrate in contact with the bottom plate acted as the lower electrode, producing the electric field across a 2 mm vacuum gap. All reflectivity was collected under vacuum (< 9 x 10^{-5} Torr) to avoid arcing when a potential was applied to the electrodes. Scans were taken first with no applied potential, then with 0.5, 2.0, 5.0, and 7.0 kV using a Trek 610E high voltage supply, corresponding to a maximum applied electric field of 3.5 V/μm.

2.4 Neutron Reflectivity Analysis. The analysis was done using the Motofit reflectivity analysis procedure[30] within Igor Pro (Wavemetrics). Error bars were obtained by propagating error using uncertainties in the SLD and thickness obtained from the Monte Carlo analysis tool in Motofit (see Supporting Information Section S2 for a detailed fitting discussion, Tables S2-4 for parameter values, and Figures S3,4 for discussions on model quality). Additionally, to further confirm the accuracy of these models, the 0 and 7 kV scans for both systems were also fit within the RasCAL fitting environment (https://sourceforge.net/projects/rscl/) using a Bayesian Markov Chain Monte Carlo algorithm[31] (Figure S5). This fitting routine independently confirmed the initial analysis done using Motofit.

2.5 Coarse-grained Model. The ionic diblock copolymer was depicted by a bead-spring chain. Each copolymer chain consisted of 150 beads with a block fraction of 0.7, so that the ionic A block contained 105 beads and the neutral B block contained 45 beads. Degree of ionization of the ionic block was set as 14.3% in this study. Specifically, the first bead in every 7 beads along the ionic block was assigned as a charged bead (cA), which carried a positive elementary charge. An equal amount of counteranions (ci) were included in the system to ensure global electroneutrality. The remaining beads in the A block were treated as neutral beads (nA). The mixture of copolymers and counteranions (with a polymer bead number density of 0.7) was confined in the z direction by two planar walls, where each comprised N_{wb} neutral beads distributed on a simple square lattice. Asymmetric wetting conditions were applied such that the B blocks selectively wetted the top surface. Periodic boundary conditions were enforced in x and y directions and a static electric field (*E*) was applied along the z direction pointing towards the bottom wall. Standard Lennard-Jones reduced units were used and all quantities were non-dimensionalized with respect to the length unit σ, energy unit ε, and mass m. The two counteranion diameters were chosen (0.46 and 0.36) correspond to the size of BF_4 and Br counteranions, respectively. For simplicity, all the neutral beads had a diameter of 1.0. Size of the pairing charged A bead for each counteranion was determined such that the total volume of the cA-ci charge pair was equal to that of a neutral bead (nA or B). Detailed force fields and parameter settings are presented in the SI.

2.6 Molecular Dynamics Simulations. The simulations were performed using the LAMMPS software package.[32] Detailed simulation procedures can be found in the SI. All the simulations were run in NVT ensemble with a Langevin thermostat. Two types of simulations were conducted, one with static and the other with mobile boundaries. In the simulations with mobile boundaries, constant non-zero forces were applied along normal to the walls (i.e., along the z-axis). In particular, magnitude of the force per bead on the wall was computed from P_{zz}·(area of the

wall)/N_{wb}, where P_{zz} is the averaged normal component of the pressure tensor for the mixture of copolymers and counteranions in the absence of an electric field (i.e., E = 0). Rather than fixing both walls during the simulations, they were allowed to move in the z direction until they reached a point where the forces balanced (cf. Figure S12 for a comparison between two types of boundaries and Figure S13 for a case study using mobile boundaries). At first, the SLD profiles were constructed using the averaged density distributions along the z-axis in the steady state from the simulations executed with static boundaries. Based on these simulations, parameters were identified, which reproduced the SLD profiles exhibiting qualitative agreements with the experimental findings at E = 0. These parameters were varied further to study the responses of the systems under applied electric fields. Specifically, the maximum film thickness changes found in the NR experiments were applied to the simulation box height h, i.e., -1.5% and 5.3% for the PIL-BCP-BF_4 and the PIL-BCP-Br, respectively, while simulating with static boundaries. The electric field strength was varied to study changes in the SLD profiles. The system configurations at E = 0 were used in the subsequent simulations executed with mobile boundaries. The temporal evolution of film thickness (i.e., the separation between the two walls) in the steady state was monitored in the simulations at different electric field strengths.

3. RESULTS AND DISCUSSION

3.1 Neutron Reflectometry (NR) under an Applied Electric Field. Diblock copolymers were synthesized with an imidazolium containing ionic block with either a tetrafluoroborate (BF_4) or bromide (Br) counteranion and a deuterated polystyrene (dPS) block, which are denoted as PIL-BCP-BF_4 and PIL-BCP-Br. In this study, a volume fraction of 0.7 for the ionic block was used to cast films with small thicknesses to achieve simple phase behavior. The two PIL-BCP films were prepared using the same spin coating conditions on silicon (Si) wafers, resulting in a slightly thicker film for PIL-BCP-Br. As mentioned previously, the presence of charged groups and counterions can alter the morphological phase diagram of block copolymers, which can be further complicated by film thickness due to phase structure commensurability.[33-34] The glass-transition temperature (T_g) was measured using differential scanning calorimetry (DSC). Two T_gs were found for both systems, which is expected for microphase separated block copolymers. The T_gs found for PIL-BCP-BF_4 were -18 and 95 °C, while T_gs for PIL-BCP-Br were -17 and 95 °C, where the lower temperatures correspond to the ionic block and the higher temperatures correspond to the styrene block.

In NR, the beam is reflected off the sample surface and the ratio of the specularly reflected beam to incident beam intensity, *i.e.* reflectivity, is plotted against the momentum transfer vector $Q_z = (4\pi\sin\theta)/\lambda$, where θ is the incident angle and λ is the wavelength of the beam. The reflectivity profiles (obtained by varying θ and λ (determined from time-of-flight)) contain information about the thickness, composition, and roughness of component layers within the film, normal to the substrate surface. The sub-nanometer resolution and non-

destructive nature of NR makes it an ideal tool for probing the electroresponsiveness in soft matter systems.[35]

The experimental setup of NR measurements on the films is illustrated in Figure 1a, where electric fields were applied normal to and directed towards the Si substrate. The collected reflectivities were modeled in Motofit[30] within Igor Pro (Wavemetrics) which employs an Abeles matrix formalism where the calculated reflectivity is based on a layered system. The thickness, roughness, and composition of each layer in the model were varied to minimize differences between the models and raw datasets as quantified by standard χ^2 distributions while maintaining physical relevance to the system (see Methods and Supporting Information for a detailed discussion of the NR analysis). In neutron studies, scattering length density (SLD) is used to represent the composition of a material through SLD = $(1/V_m)\,\Sigma b_i$, where V_m is the molecular volume and b_i is the coherent scattering length of atom i in the material. The use of deuterated PS provides contrast between the two polymer blocks in the NR measurements as the neutron coherent scattering length of deuterium is significantly different than that of hydrogen (6.671 fm and -3.741 fm, respectively[36]). Figure 1b,c show the reflectivity curves and variation of SLD as a function of film depth, which provides information on compositional variation within the polymer films due to the applied electric field strengths.

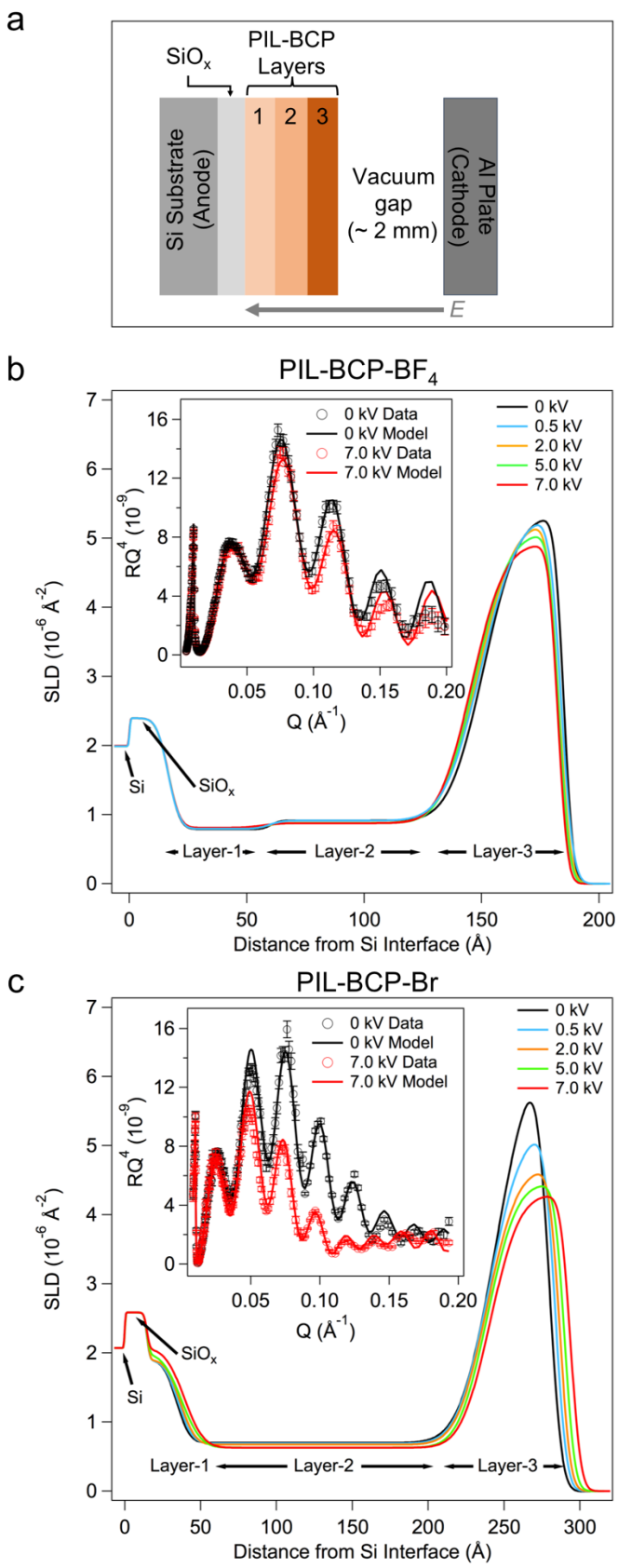
a
SiOx
PIL-BCP Layers
1
2
3
Si Substrate (Anode)
Vacuum gap (~ 2 mm)
Al Plate (Cathode)
E
b
PIL-BCP-BF4
0 kV
0.5 kV
2.0 kV
5.0 kV
7.0 kV
0 kV Data
0 kV Model
7.0 kV Data
7.0 kV Model
RQ4 (10-9)
Q (Å-1)
SLD (10-6 Å-2)
Si
SiOx
Layer-1
Layer-2
Layer-3
Distance from Si Interface (Å)
c
PIL-BCP-Br
0 kV
0.5 kV
2.0 kV
5.0 kV
7.0 kV
0 kV Data
0 kV Model
7.0 kV Data
7.0 kV Model
RQ4 (10-9)
Q (Å-1)
SLD (10-6 Å-2)
SiOx
Si
Layer-1
Layer-2
Layer-3
Distance from Si Interface (Å)

Figure 1. a) Schematic diagram of the experimental system, where voltages were applied over a 2 mm vacuum gap. Profiles showing the SLD as a function of distance from the Si surface for the films containing PIL-BCP-BF_4 b) and PIL-BCP-Br c) at various applied potentials. The insets show reflectivity data (open symbols) and fits (solid lines) for the 0 and 7 kV scans. Reflectivity data and fits for the 0.5, 2.0, and 5.0 kV scans (Figure S2), model parameters and uncertainties (Tables S2-3), χ^2 distribution values (Table S4), and a comprehensive discussion of the fitting procedure are included in the Supporting Information. The SLD values of individual species are 0.79, 0.70, and 6.42 in units of 10^{-6} $Å^{-2}$ for ionic block-BF_4, ionic block-Br, and dPS, respectively.

In Figure 1b, the SLD profiles demonstrated the presence of three distinct domains/layers normal to the Si wafer in the PIL-BCP-BF_4 film. In the absence of an applied electric field, Layer-1 at the SiO_x interface comprised ionic block of the polymer; the intermediate Layer-2 had a slightly higher SLD, attributed to the presence of dPS; and Layer-3 at the air interface was dominated by dPS as evidenced by the large increase in SLD. The SLD profile implies that the PIL-BCP-BF_4 system had a lamellar-like structure with a *diffuse* interface between ionic and neutral blocks in the thin film. The ionic block preferentially wetted the Si wafer and the hydrophobic dPS largely segregated to the air interface.

In Figure 1c, the SLD profile for the PIL-BCP-Br film revealed a slightly different structure in the absence of an electric field. Specifically, dPS was found to be mixed with the ionic block in Layer-1, close to the Si interface, leading to an increase in SLD, while Layer-2 consisted only of ionic block. These differences in structure of the PIL-BCP-BF_4 and PIL-

BCP-Br films were mainly caused by the change in film thickness.[34, 37] With an increase in thickness, copolymer chains tend to form more lamellar domains to avoid stretching. The presence of neutral blocks near Si surface in PIL-BCP-Br films is expected by this argument. One would expect that the PIL-BCP-BF_4 film would adopt a similar structure with dPS near the Si interface as film thickness increased as well. Additionally, a steeper slope for the interface between Layer-2 and -3 was seen for the PIL-BCP-Br, indicating a sharper interface between neutral and ionic blocks and hence a larger segregation strength in the PIL-BCP-Br system.

Under an applied electric field, the general shape of SLD profiles remained the same in both thin films. A similar trend was found in both systems as the magnitude of SLD decreased in Layer-3 and Layer-2 while increased in Layer-1 as the field strength increased. Additionally, Layer-1 contracted in the PIL-BCP-BF_4 film while it expanded in the PIL-BCP-Br film, resulting in contrasting behavior in overall film thickness changes. This finding was consistent with an estimate for total film thickness ($d = 2\pi/\Delta q$) obtained by measuring the Kiessig fringe spacing (Δq) from the raw reflectivity data. Also, the estimate was consistent with the SLD profiles corresponding to the best fits of the reflectivities and revealed a maximum 1.5% contraction and 5.3% expansion in the films containing BF_4 and Br counteranions, respectively.

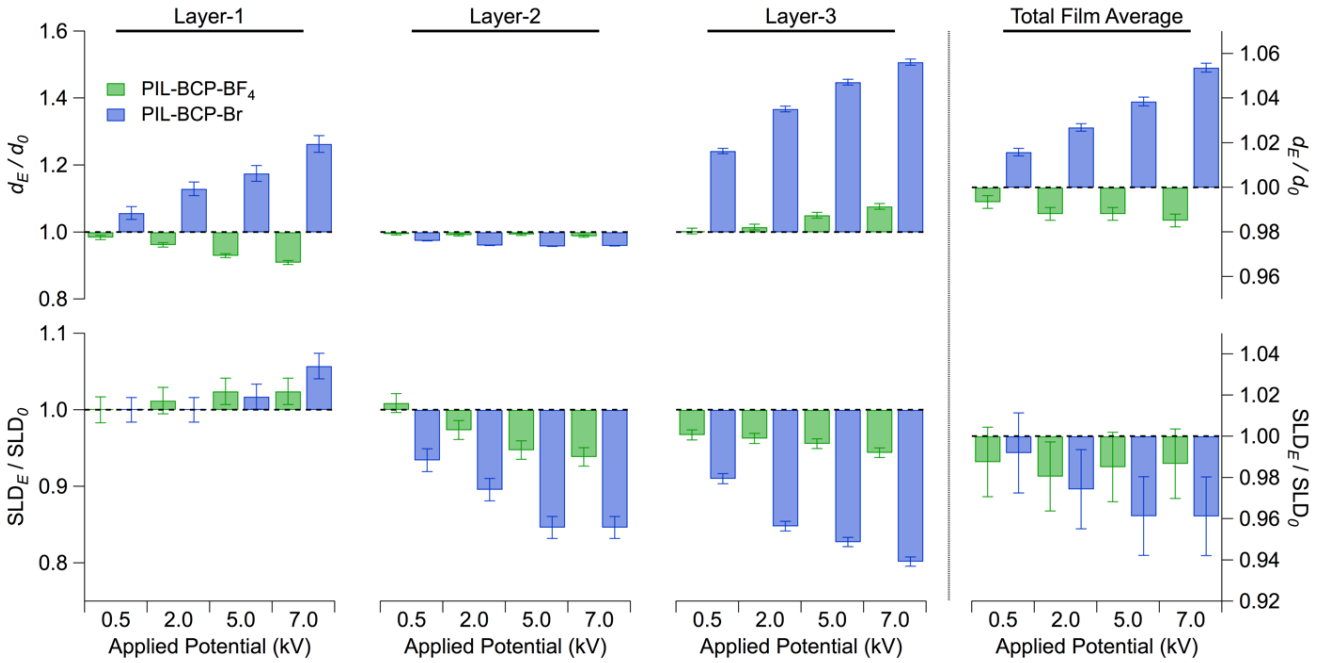

Figure 2. Ratios of thickness (top row) and SLD (bottom row) between the presence (*E*) and absence (*0*) of applied electric potentials for thin films containing PIL-BCP-BF_4 (green) and PIL-BCP-Br (blue). Mass movement analysis is included in Figure S6.

Ratios for the thickness (d_E/d_0) and SLD (SLD_E/SLD_0) of the *individual* film layers, which quantify local changes caused by the electric field, are shown in Figure 2. Here, subscript *E* indicates the presence of an applied electric field and *0* corresponds to the absence. It is manifest that the PIL-BCP-Br film exhibited larger variations in both thickness and SLD throughout the film as the strength of applied electric field was increased. Note that the Br counteranion has a much smaller coherent scattering length (b_{Br}=6.79 fm) than BF_4 (b_{BF4}=27.9 fm), and so, the same amount of counteranion mass movement would show a smaller effect on changes in SLD for the Br system. Thus, the comparatively larger changes in SLD indicate that the PIL-BCP-Br film had been subjected to more mass exchange than the PIL-BCP-BF_4 film.

As each thin film comprised three mobile components (ionic block, dPS, and counteranions), it is difficult to deconvolute these results further and understand the motion of individual components in the presence of an electric field. To gain deeper insights into the motion of individual components and decipher the origin of the contrasting behavior between the two types of films in similar field strengths, molecular dynamics simulations based on coarse-grained models were executed. Two types of simulation strategies were employed to develop a comprehensive understanding of the electroresponsiveness in the films. First, thin films with static boundaries were simulated to justify the parameter choice in simulations regarding the experimental findings; later, confining boundaries were allowed to move in response to the applied electric field *E*, presenting the corresponding changes in film thickness.

3.2 Molecular Dynamics (MD) Simulations with Static Boundaries. The coarse-grained models (see details in the SI) contained six types of particles. Each ionic diblock copolymer was depicted by a bead-spring chain. The ionic block consisted of neutral A (nA) and charged A (cA) beads while the neutral block (representing dPS) was made of connected neutral B beads. Counteranions (ci) were included to preserve overall electroneutrality. Film confinement was enforced by simulating additional boundary particles representing the Si substrate and the air surface, labeled as bottom wall (bW) and top wall (tW), respectively. Standard Lennard-Jones reduced units were adopted and box sizes normal to the Si substrate were mapped to the thin films studied in experiments using a length unit σ=1nm. Two types of counteranions were considered in

the model thin films, with diameters R_{ci}=0.46 and 0.36, representing BF_4 and Br, respectively. These diameters were chosen based on reported values.[38-39]

Aside from the Coulombic forces, the pair interactions among all the beads were purely repulsive. The force fields of the two counteranion systems were identical except for the interaction parameter between B and ci, ε_{Bci}, which was distinguished to take into account the ion-specific solvation effect[11, 40-41] in an *ad hoc* manner. Specifically, ε_{Bci}=1.0 and 4.0 in systems of BF_4 and Br, respectively. A larger interaction parameter ε_{Bci} was used for the smaller counteranion Br, which characterizes stronger repulsive interactions between ci and B beads. Hence, it is relatively harder for the smaller counteranions to enter B domains, which is qualitatively similar to the energy barrier for crossing domains due to the Born solvation energy ($u = \frac{e^2}{4\pi R_{ci}\varepsilon_0\varepsilon_r}$, e is the elementary charge, ε_0 is vacuum permittivity, and ε_r is dielectric constant).[40-41] We note that the variation of ε_{Bci} does not change the copolymer phase behavior and the qualitative thin film response to the applied electric field, as will be discussed in a following section.

The SLD profiles were constructed using the averaged particle number density distributions normal to the substrate in the steady state (see details in the SI). Qualitative agreement between computed SLD profiles and the experimental results (Figure 1) were taken as criteria for the choice of parameters. Figure 3a-d displays a typical set of simulation snapshots for two films at E = 0 and 0.01 (cf. Figure S10 for density distributions and Figure S11 for computed SLD profiles). Under the confinement and selective surface wetting conditions, the film containing counteranions of R_{ci}=0.46 (PIL-

BCP-BF_4) exhibited a lamellar structure at E = 0 (Figure 3a), while the film containing counteranions of R_{ci}=0.36 (PIL-BCP-Br) showed a slightly different morphology (Figure 3c), with the presence of B near the bottom (as inferred from Figure 1b). Notice that neutron reflectivity provides laterally averaged information about the morphological behavior, Figure 3a,c presents thermodynamically consistent models for these thin films (which were verified by simulations from different initial configurations). At E = 0.01 (Figure 3b,d), the overall symmetries of the morphologies were largely maintained while the relocation of B beads under electric field to the lower domain was observed.

Differences in local number densities of individual components ($\Phi_E - \Phi_0$) in the presence and absence of electric field are shown in Figure 3e,f, providing information of mass transfer for each particle species under electric field E = 0.01. Counteranions moved opposite to the direction of the electric field and a portion of charged A particles *also moved with them* due to strong electrostatic correlations, rendering a negative transference number (which has been measured experimentally[42]). The neutral B beads migrated along a direction opposite to the motion of A (ionic blocks) to satisfy the incompressibility constraint. This motion of B explains the decrease in experimental SLD in Layer-3 and the corresponding increase in Layer-1 seen in both systems (Figure 2). Moreover, Figure 3e,f shows that the magnitude of changes in density distribution were much larger in the PIL-BCP-Br system, qualitatively capturing the main features of the NR measurement results.

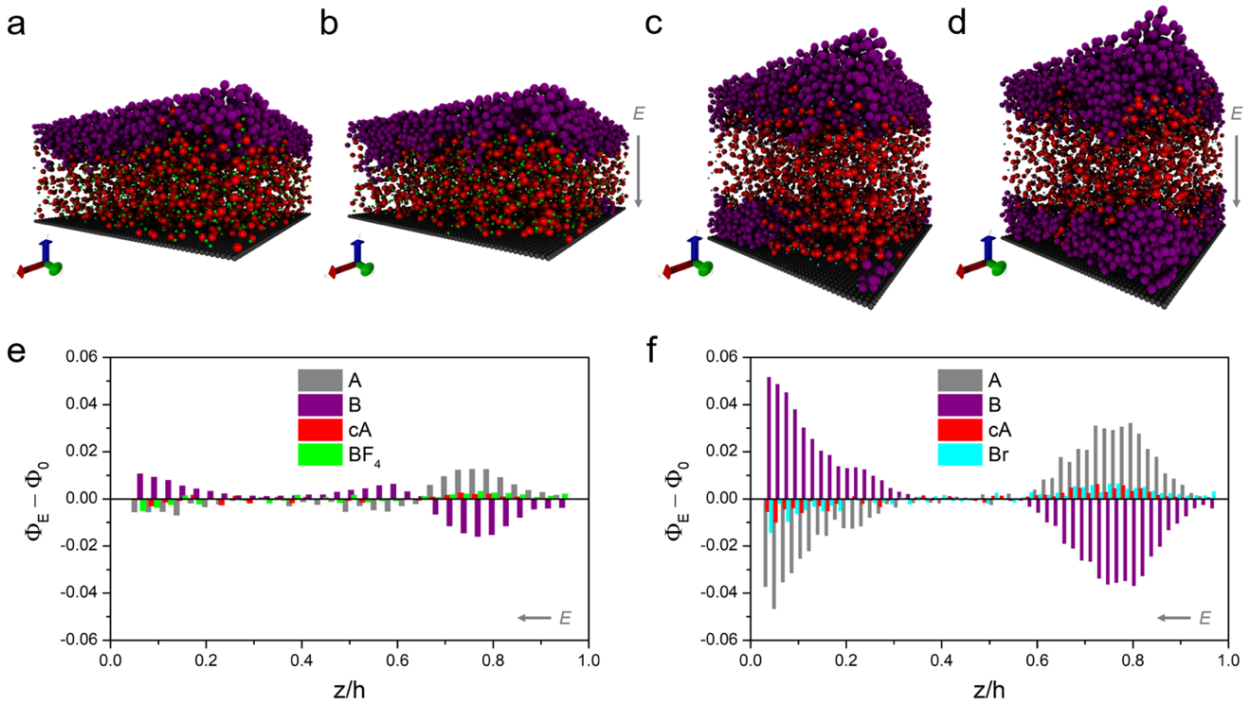

Figure 3. MD snapshots of the R_{ci}=0.46 (PIL-BCP-BF_4) system at a) E = 0 and b) E = 0.01 (film thickness h = 16.85 and 16.60). Snapshots of the R_{ci}=0.36 (PIL-BCP-Br) system at c) E = 0 and d) E = 0.01 (film thickness h = 26.50 and 27.90). B beads are colored in purple and charged A beads are in red. The BF_4 and Br counteranions are colored in green and cyan, respectively. Black beads represent the bottom wall (silicon substrate). Neutral A beads are not shown for clarity. Configurations at different parameter settings can be found in Figure S8 and the associated radial distribution functions between charged A beads and counteranions are included in Figures S7 and S9. e,f) Number density (Φ) differences along the z direction (normalized by the film thickness h) between rescaled density profiles of E = 0.01 and E = 0.0 (enforcing system incompressibility and ignoring film thickness changes) in the corresponding thin films, which reveal movement of different types of particles under electric field. Bin size is approximately 0.5.

3.3 MD Simulations with Mobile Boundaries. The MD simulations with static boundaries demonstrated the validity of the adopted coarse-grained model for capturing the essential physics in the experimental systems and provided details related to the motion of different components that give rise to the observed changes in the SLD profiles under applied electric fields. However, these simulations provided no direct information about the underlying mechanism of film thickness change. To further investigate the mechanism of film contraction or expansion in response to the electric field, MD simulations utilizing mobile boundaries were performed for the same model systems discussed above. For comparison, another system, PIL-BCP-CG, was introduced, which was identical to PIL-BCP-BF_4 except a larger interaction parameter, ε_{Bci}=4.0, was used. This difference did not change the system phase behavior in the simulations. We note that despite the slight morphological difference between PIL-BCP-BF_4 and PIL-BCP-Br due to film thickness, the main characteristics of lamellar domain structures and electroresponsiveness to the applied electric field were the same. Collectively, these three systems allow the interrogation of both counteranion size and interaction parameter effects.

Figure 4a shows the changes in film thickness as a function of applied electric field strength. With increasing *E*, the film thickness decreased first and then increased for PIL-BCP-BF_4 and PIL-BCP-CG, exhibiting a non-monotonic trend. For PIL-BCP-Br, a similar trend was observed while the overall film decrease was negligible. These results suggest that the NR experimental setup may correspond to a region where the PIL-BCP-BF_4 film is still in the contraction regime that only exhibits a monotonic decrease in film thickness,

while the PIL-BCP-Br film shows expansion. Nevertheless, the MD results indicate that thin films containing the ionic diblock copolymers should eventually expand under a sufficiently large *E*, irrespective of counteranion identity. Unfortunately, this prediction was not verified from the experiments, owing to limitations on the maximum voltage that could be applied.

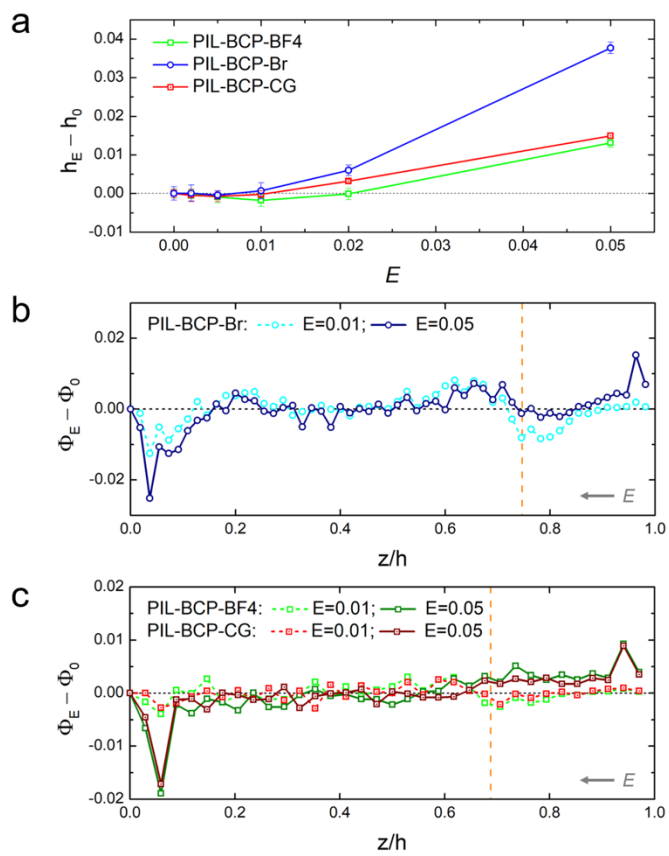

Figure 4. a) Film thickness variation as a function of electric field strength. Error bars were obtained from window averaging. b,c) Depth profiles for the number density differences ($\Phi_E - \Phi_0$) of the counteranions resulting from their movement along z (normalized by the film thickness h) at E = 0.01 and 0.05 in the thin films containing ions of sizes R_{ci}=0.36 and 0.46, respectively. Vertical dashed lines (approximately) indicate the interface between the A domain and top B domain (cf. Figure S10).

Counteranion identity affects the dependence of total film thickness on *E*, which determines the range of applied electric field strengths over which the contraction was observed, as well as the magnitude of maximum contraction. Comparing PIL-BCP-BF_4 and PIL-BCP-CG, the thickness variation curve shifts upwards as ε_{Bci} increases, which renders a shallower well in the curve and hence a smaller film contraction window in *E*. This trend appears to be further promoted by the decrease in counteranion size that makes the film expansion under electric field more dominant for PIL-BCP-Br.

The non-monotonic changes in total film thickness, specifically the initial decrease, was accompanied by a redistribution of counteranions in the applied fields. At $E = 0$, a few counteranions populated the B domains due to entropic effects, resulting in a small local charge imbalance such that the B domains were net negatively charged while the A domains were positively charged (cf. Figure S10). Under an applied electric field, translation of the counteranions in a direction opposite to the applied electric field led to gradual accumulation of charges at two boundary surfaces. As an illustration, the changes in counteranion distribution in the three films for different values of *E* are shown in Figure 4b,c.

Figure 4b shows the depth profile of relative counteranion movement at $E = 0.01$ and 0.05 in the PIL-BCP-Br film. At $E = 0.01$, counteranions were moved away from the interface (vertical dashed line) mostly into the A domain. At $E = 0.05$, more counteranions from the A domain entered the top B domain due to stronger ion-pair dissociation. The same trends are found in Figure 4c for the systems of R_{ci}=0.46. Comparatively, larger

counteranion size and greater ε_{Bci}, diminished counteranion movement, indicating that it is easier for the electric field to reorganize the smaller counteranions, while the repulsion between B and ci (ε_{Bci}) acts to hinder such ion reorganization.

3.4 Discussion and Outlook. Changes in film thickness result from variations in underlying copolymer chain stretching or contraction in the presence of an electric field. The theory for polymers in the strong-stretching regime[43-44] relates the extent of chain stretching to the interfacial tension between polymer-polymer interfaces. For *neutral* AB diblock copolymers, the chain stretching in a lamellar morphology is proportional to ${\gamma_{AB}}^{1/3}$ $N^{2/3}$, where γ_{AB} is the interfacial tension (per unit area) dictated by the immiscibility between A and B blocks, and *N* is the degree of polymerization. By extending this result to weakly charged lamellar-forming ionic diblock copolymers, it can be readily shown[45] that the chain stretching is proportional to $(\gamma_{AB} + \gamma_{ionic})^{1/3} N^{2/3}$, where γ_{ionic} is the electrostatic contribution to the interfacial tension and is additive to the interfacial tension contributions from non-electrostatic interactions. Taking γ_{AB} as invariant under a weak electric field, thickness changes in the ionic block copolymer thin films could therefore be attributed to variations in γ_{ionic} at the polymer-polymer interfaces. Thus, non-monotonic changes in the film thickness imply that γ_{ionic} should decrease first and then increase with increasing *E*.

To understand the suggested non-monotonic dependence of γ_{ionic} on *E*, an analogy between the microphase separated A-B lamellar domains under weak applied electric field and two dilute electrolyte solutions separated by a planar interface *in the absence of*

applied field is invoked. Recalling a large body of theoretical and experimental work related to the interfacial tension of electrolyte solutions, dependence of γ_{ionic} on *E* and its connection with counteranion redistribution can be inferred. Specifically, as per the classic Verwey-Niessen model,[46] ion partitioning in two solutions resulting from an electrostatic potential difference on the two sides far away from the interface leads to electrical double layers at the liquid-liquid interface. The excess interfacial tension can be calculated from the ion density profiles derived from the Verwey-Niessen model (e.g., using the Gibbs adsorption isotherm[47]), and decreases with increasing salt concentration (cf. Supporting Information Section S5). In addition, ion depletion from the interface, such as caused by image charge repulsion[48] and specific ion-interface interactions,[49] would lead to an increase in interfacial tension, as delineated by the Onsager-Samaras limiting law.[48, 50] The collective effect of these two competing factors could result in a nonmonotonic change in interfacial tension as a function of salt concentration. Such a phenomenon was first observed experimentally by Jones and Ray.[51] The development of a unified theory for the interfacial tension which captures all of the effects remains an active research topic.[50, 52-56]

We note that applying voltage bias across the ionic diblock copolymer film causes the counteranion redistribution and the build-up of electrical double layer around the A-B interface. The system under weak electric field essentially resembles an electrolyte solution in the low salt concentration limit. Increasing the voltage bias imparts a similar effect as adding salt into the solutions. Such a resemblance between ion concentration and potential difference implies that the non-monotonic change in γ_{ionic} on varying *E*, *i.e.*,

γ_{ionic} decreases first and then increases as *E* is increased, is induced by the counteranion redistribution around the polymer-polymer interface under the applied electric field. As a consequence, the thickness change under weak electric fields for the ionic diblock copolymer thin films with specific structures should follow the same trend as captured by the Jones-Ray effect[51] and the specific ion effect[55] in electrolyte solutions. As the electric field strength increases further, additional effects related to electrostatic coupling with chain conformation and thin film confinement emerge due to significant ion-pair dissociation.[22] When strong electric fields are applied, effects such as electrostatic repulsions among the charged groups on polymer chains and build-up of electrostatic pressure (i.e., Maxwell stress) at both boundaries, could also contribute to the film expansion.

In addition to the applied potential difference across the films, dielectric heterogeneity can also regulate ion partitioning in different domains,[56] yielding an important parameter to control the behavior of γ_{ionic} and film thickness response. In the simulations, dielectric mismatch between ionic and non-ionic blocks was not included while effects of ion solvation and polarizability were considered phenomenologically by varying the interaction parameter ε_{Bci}. We expect that dielectric mismatch could modify the electric field dependence observed here and lead to an additional parametric dependence. Including local dielectric constants self-consistently and the inclusion of dielectric mismatch in molecular dynamics simulations remains a challenge and are not expected to play an important role until much stronger electric fields than those employed in this study are explored. Under high applied electric fields, the effects of local dielectric

constants could result in phase morphology alignments[57] as well as phase transitions.[58-59] The complexity of copolymer morphological behavior at large *E* with properly incorporated dielectric heterogeneity along with the inclusion of ionic species would further enrich the phenomenon of electroresponsiveness, providing an interesting avenue for future studies.

In summary, the present work employed PIL-BCPs that underwent small ion dissociation and employed weak electric fields under ambient temperatures, ultimately exposing a response mechanism that has been unobserved in previous studies due to the use of high electric fields or temperatures above polymer T_gs. The experimental results provide two cases (contraction and expansion) and the combined picture corroborates the counteranion dependent non-monotonic film thickness behavior observed in the MD simulations. This qualitative agreement highlights the dominant effects of counteranion redistribution (ion partitioning) under weak electric fields in PIL-BCPs, providing a promising route towards achieving the ability to tune the response of these materials for specific applications. The general nature of the analysis discussed above suggests that the non-monotonic dependence of *E* should exist in other ionic block copolymer films exhibiting interfaces between ionic and non-ionic domains. Given the rich behavior of counteranion identity (e.g., Hofmeister Series[55] in co-existing electrolyte solutions), a similar behavior for PIL-BCP lamellar films could be expected. The complexity of this non-monotonic behavior needs to be explored in future theoretical developments, experimental examinations, and simulation studies.

4. CONCLUSION

This work presents a direct observation of electric field induced motion of ionic diblock copolymer thin films with nanoscale resolution. Neutron reflectometry was used to determine the effect of counteranion identity on the response of ionic diblock copolymers to external electric fields. The modeled reflectivity data demonstrated that the choice of counteranion leads to different changes in film thickness. Specifically, the thin film containing BF_4 experienced contraction in the tested range of applied electric fields, while the thin film containing Br underwent expansion. A coarse-grained simulation model calibrated with the experimental findings further uncovered a general non-monotonic trend in film thickness response as well as the effect of counteranion identity, which closely resembles the Jones-Ray effect and the specific ion effect. To the best of our knowledge, the presented results are the first reported instance of this non-monotonic behavior in polymeric systems, which reveal the importance of coupling between counteranions and copolymer phase morphology in affecting the electroresponsiveness of ionic block copolymers under applied electric field. The relevance of the findings pertains to the deployment of ionic copolymer systems in engineering applications (energy storage, transducers, flexible electronics, etc.) commonly operated under ambient temperatures and under relatively low applied voltages, as choice of counterion in these systems could alter their mechanical response and hence, efficiency, performance lifetime, and operating safety. Furthermore, this work highlights the potential mechanistic insights to be gained when experimental and computational approaches

converge on length scales relevant to establishing a nanoscale understanding of the underlying processes.

Supporting Information

Details on the block copolymer composition, neutron reflectometry fitting and analysis, force fields and molecular dynamics procedures, as well as ancillary computational results and discussion.

Author Contributions

J.W.D., B.S.L., and J.F.B. conducted the NR experiments at both SNS and ISIS. W.L. and R.K. designed the coarse-grained model and made theoretical analysis. W.L. performed the MD simulations. M.C. synthesized the polymers under the guidance of T.E.L. and B.S.L.. R.J.L.W. and M.W.A.S. assisted with the NR experiments at RAL. J.W.D. and W.L. drafted the manuscript. B.S.L., R.K., and J.F.B. supervised the research. All authors contributed to the discussion and writing of the paper.

Notes

The authors declare no competing financial interests.

ACKNOWLEDGEMENTS

This research was supported by Oak Ridge National Laboratory's (ORNL) Laboratory Directed Research and Development Program. Work was conducted at the Center for Nanophase Materials Sciences and the Spallation Neutron Source, which are US Department of Energy Office of Science User Facilities. We gratefully acknowledge the Science and Technology Facilities Council (STFC) for access to neutron beam time conducted at ISIS, data available at DOI: 10.5286/isis.e.84782763. The authors are grateful to P. Bonnesen for assistance with the 13C NMR measurements and D. Uhrig for aiding with SEC.

REFERENCES

1. Armand, M.; Tarascon, J. M., Building Better Batteries. *Nature* **2008,** *451*, 652-657.

2. Hallinan, D. T.; Balsara, N. P., Polymer Electrolytes. *Annu. Rev. Mater. Res.* **2013,** *43*, 503-525.

3. Ueki, T.; Watanabe, M., Macromolecules in Ionic Liquids: Progress, Challenges, and Opportunities. *Macromolecules* **2008,** *41*, 3739-3749.

4. Meek, K. M.; Elabd, Y. A., Polymerized Ionic Liquid Block Copolymers for Electrochemical Energy. *J. Mater. Chem. A* **2015,** *3*, 24187-24194.

5. Wang, X. J.; Goswami, M.; Kumar, R.; Sumpter, B. G.; Mays, J., Morphologies of Block Copolymers Composed of Charged and Neutral Blocks. *Soft Matter* **2012,** *8*, 3036-3052.

6. Teran, A. A.; Balsara, N. P., Thermodynamics of Block Copolymers with and without Salt. *J. Phys. Chem. B* **2014,** *118*, 4-17.

7. Marko, J. F.; Rabin, Y., Microphase Separation of Charged Diblock Copolymers: Melts and Solutions. *Macromolecules* **1992,** *25*, 1503-1509.

8. Kumar, R.; Muthukumar, M., Microphase Separation in Polyelectrolytic Diblock Copolymer Melt: Weak Segregation Limit. *J. Chem. Phys.* **2007,** *126*, 214902.

9. Sing, C. E.; Zwanikken, J. W.; Olvera de la Cruz, M., Electrostatic Control of Block Copolymer Morphology. *Nat. Mater.* **2014,** *13*, 694-698.

10. Ye, Y.; Choi, J.-H.; Winey, K. I.; Elabd, Y. A., Polymerized Ionic Liquid Block and Random Copolymers: Effect of Weak Microphase Separation on Ion Transport. *Macromolecules* **2012,** *45*, 7027-7035.

11. Nakamura, I.; Balsara, N. P.; Wang, Z. G., Thermodynamics of Ion-Containing Polymer Blends and Block Copolymers. *Phys. Rev. Lett.* **2011,** *107*, 198301.

12. Amundson, K.; Helfand, E.; Davis, D. D.; Quan, X.; Patel, S. S.; Smith, S. D., Effect of an Electric Field on Block Copolymer Microstructure. *Macromolecules* **1991,** *24*, 6546-6548.

13. Morkved, T. L.; Lu, M.; Urbas, A. M.; Ehrichs, E. E.; Jaeger, H. M.; Mansky, P.; Russell, T. P., Local Control of Microdomain Orientation in Diblock Copolymer Thin Films with Electric Fields. *Science* **1996,** *273*, 931-933.

14. Gurovich, E., On Microphase Separation of Block Copolymers in an Electric Field: Four Universal Classes. *Macromolecules* **1994,** *27*, 7339-7362.

15. Lin, C.-Y.; Schick, M.; Andelman, D., Structural Changes of Diblock Copolymer Melts Due to an External Electric Field: A Self-Consistent-Field Theory Study. *Macromolecules* **2005,** *38*, 5766-5773.

16. Matsen, M. W., Stability of a Block-Copolymer Lamella in a Strong Electric Field. *Phys. Rev. Lett.* **2005,** *95*, 258302.

17. Tsori, Y.; Tournilhac, F.; Leibler, L., Demixing in Simple Fluids Induced by Electric Field Gradients. *Nature* **2004,** *430*, 544-547.

18. Tsori, Y.; Tournilhac, F.; Andelman, D.; Leibler, L., Structural Changes in Block Copolymers: Coupling of Electric Field and Mobile Ions. *Phys. Rev. Lett.* **2003,** *90*, 145504.

19. Tsori, Y.; Tournilhac, F.; Leibler, L., Orienting Ion-Containing Block Copolymers Using Ac Electric Fields. *Macromolecules* **2003,** *36*, 5873-5877.

20. Tsori, Y.; Leibler, L., Phase-Separation in Ion-Containing Mixtures in Electric Fields. *Proc. Natl. Acad. Sci. U.S.A.* **2007,** *104*, 7348-7350.

21. Kaiser, V.; Bramwell, S. T.; Holdsworth, P. C.; Moessner, R., Onsager's Wien Effect on a Lattice. *Nat. Mater.* **2013,** *12*, 1033-7.

22. Kumar, R.; Bocharova, V.; Strelcov, E.; Tselev, A.; Kravchenko, II; Berdzinski, S.; Strehmel, V.; Ovchinnikova, O. S.; Minutolo, J. A.; Sangoro, J. R.; Agapov, A. L.; Sokolov, A. P.; Kalinin, S. V.; Sumpter, B. G., Ion Transport and Softening in a Polymerized Ionic Liquid. *Nanoscale* **2015,** *7*, 947-955.

23. Onsager, L.; Kim, S. K., Wien Effect in Simple Strong Electrolytes. *J. Phys. Chem.* **1957,** *61*, 198-215.

24. Thurn-Albrecht, T.; DeRouchey, J.; Russell, T. P.; Jaeger, H. M., Overcoming Interfacial Interactions with Electric Fields. *Macromolecules* **2000,** *33*, 3250-3253.

25. Wojnarowska, Z.; Feng, H.; Fu, Y.; Cheng, S.; Carroll, B.; Kumar, R.; Novikov, V. N.; Kisliuk, A. M.; Saito, T.; Kang, N.-G.; Mays, J. W.; Sokolov, A. P.; Bocharova, V., Effect of Chain Rigidity on the Decoupling of Ion Motion from Segmental Relaxation in Polymerized Ionic Liquids: Ambient and Elevated Pressure Studies. *Macromolecules* **2017,** *50*, 6710-6721.

26. Thelen, J. L.; Inceoglu, S.; Venkatesan, N. R.; Mackay, N. G.; Balsara, N. P., Relationship between Ion Dissociation, Melt Morphology, and Electrochemical Performance of Lithium and Magnesium Single-Ion Conducting Block Copolymers. *Macromolecules* **2016,** *49*, 9139-9147.

27. Wang, R.-Y.; Guo, X.-S.; Fan, B.; Zou, S.-F.; Cao, X.-H.; Tong, Z.-Z.; Xu, J.-T.; Du, B.-Y.; Fan, Z.-Q., Design and Regulation of Lower Disorder-to-Order Transition Behavior in the Strongly Interacting Block Copolymers. *Macromolecules* **2018,** *51*, 2302-2311.

28. Brown, J. R.; Seo, Y.; Hall, L. M., Ion Correlation Effects in Salt-Doped Block Copolymers. *Phys. Rev. Lett.* **2018,** *120*, 127801.

29. Chen, M. T.; Dugger, J. W.; Li, X. L.; Wang, Y. Y.; Kumar, R.; Meek, K. M.; Uhrig, D. W.; Browning, J. F.; Madsen, L. A.; Long, T. E.; Lokitz, B. S., Polymerized Ionic Liquids: Effects of Counter-Anions on Ion Conduction and Polymerization Kinetics. *J. Polym. Sci., Part A: Polym. Chem.* **2018,** *56*, 1346-1357.

30. Nelson, A., Co-Refinement of Multiple-Contrast Neutron/X-Ray Reflectivity Data Using Motofit. *J. Appl. Crystallogr.* **2006,** *39*, 273-276.

31. Haario, H.; Laine, M.; Mira, A.; Saksman, E., Dram: Efficient Adaptive Mcmc. *Stat. Comput.* **2006,** *16*, 339-354.

32. Plimpton, S., Fast Parallel Algorithms for Short-Range Molecular-Dynamics. *J. Comp. Phys.* **1995,** *117*, 1-19.

33. Knoll, A.; Horvat, A.; Lyakhova, K. S.; Krausch, G.; Sevink, G. J. A.; Zvelindovsky, A. V.; Magerle, R., Phase Behavior in Thin Films of Cylinder-Forming Block Copolymers. *Physical Review Letters* **2002,** *89*, 035501.

34. Segalman, R. A., Patterning with Block Copolymer Thin Films. *Mater. Sci. Eng. R Rep.* **2005,** *48*, 191-226.

35. Torikai, N.; Yamada, N. L.; Kawaguchi, D.; Takano, A.; Matsushita, Y.; Watkins, E.; Majewski, J. P., Depth Distribution of Different Solvents in a Phase-Separated Block Copolymer Thin Film. *J. Phys. Conf. Ser.* **2011,** *272*.

36. Sears, V. F., Neutron Scattering Lengths and Cross Sections. *Neutron News* **1992,** *3* , 26-37.

37. Knoll, A.; Horvat, A.; Lyakhova, K. S.; Krausch, G.; Sevink, G. J.; Zvelindovsky, A. V.; Magerle, R., Phase Behavior in Thin Films of Cylinder-Forming Block Copolymers. *Phys. Rev. Lett.* **2002,** *89*, 035501.

38. Li, P.; Paul, D. R.; Chung, T. S., High Performance Membranes Based on Ionic Liquid Polymers for Co2 Separation from the Flue Gas. *Green Chem.* **2012,** *14*, 1052-1063.

39. Bondi, A., Van Der Waals Volumes and Radii. *J. Phys. Chem.* **1964,** *68*, 441-451.

40. Wang, Z. G., Fluctuation in Electrolyte Solutions: The Self Energy. *Phys. Rev. E Stat. Nonlin. Soft Matter Phys.* **2010,** *81*, 021501.

41. Nakamura, I.; Shi, A. C.; Wang, Z. G., Ion Solvation in Liquid Mixtures: Effects of Solvent Reorganization. *Phys. Rev. Lett.* **2012,** *109*, 257802.

42. Pesko, D. M.; Timachova, K.; Bhattacharya, R.; Smith, M. C.; Villaluenga, I.; Newman, J.; Balsara, N. P., Negative Transference Numbers in Poly(Ethylene Oxide)-Based Electrolytes. *J. Electrochem. Soc.* **2017,** *164*, E3569-E3575.

43. Semenov, A. N., Theory of Block Copolymer Interfaces in the Strong Segregation Limit. *Macromolecules* **1993,** *26*, 6617-6621.

44. Ohta, T.; Kawasaki, K., Equilibrium Morphology of Block Copolymer Melts. *Macromolecules* **1986,** *19*, 2621-2632.

45. Nyrkova, I. A.; Khokhlov, A. R.; Doi, M., Microdomain Structures in Polyelectrolyte Systems: Calculation of the Phase Diagrams by Direct Minimization of the Free Energy. *Macromolecules* **1994,** *27*, 4220-4230.

46. Verwey, E. J. W.; Niessen, K. F., XI. The Electrical Double Layer at the Interface of Two Liquids. *Lond. Edinb. Dubl. Phil. Mag. J. Sci.* **1939,** *28*, 435-446.

47. Nichols, A. L.; Pratt, L. R., Salt Effects on the Surface Tensions of Dilute Electrolyte Solutions: The Influence of Nonzero Relative Solubility of the Salt between the Coexisting Phases. *The Journal of Chemical Physics* **1984,** *80*, 6225-6233.

48. Onsager, L.; Samaras, N. N. T., The Surface Tension of Debye- Hückel Electrolytes. *J. Chem. Phys.* **1934,** *2*, 528-536.

49. Markovich, T.; Andelman, D.; Podgornik, R., Surface Tension of Acid Solutions: Fluctuations Beyond the Nonlinear Poisson-Boltzmann Theory. *Langmuir* **2017,** *33*, 34-44.

50. Levin, Y.; dos Santos, A. P.; Diehl, A., Ions at the Air-Water Interface: An End to a Hundred-Year-Old Mystery? *Phys. Rev. Lett.* **2009,** *103*, 257802.

51. Jones, G.; Ray, W. A., The Surface Tension of Solutions of Electrolytes as a Function of the Concentration. I. A Differential Method for Measuring Relative Surface Tension. *J. Am. Chem. Soc.* **1937,** *59*, 187-198.

52. Bier, M.; Zwanikken, J.; van Roij, R., Liquid-Liquid Interfacial Tension of Electrolyte Solutions. *Phys. Rev. Lett.* **2008,** *101*, 046104.

53. Markovich, T.; Andelman, D.; Podgornik, R., Surface Tension of Electrolyte Interfaces: Ionic Specificity within a Field-Theory Approach. *J. Chem. Phys.* **2015,** *142*, 044702.

54. Onuki, A., Surface Tension of Electrolytes: Hydrophilic and Hydrophobic Ions near an Interface. *J. Chem. Phys.* **2008,** *128*, 224704.

55. Petersen, P. B.; Saykally, R. J., On the Nature of Ions at the Liquid Water Surface. *Annu. Rev. Phys. Chem.* **2006,** *57*, 333-364.

56. Wang, R.; Wang, Z. G., Effects of Ion Solvation on Phase Equilibrium and Interfacial Tension of Liquid Mixtures. *J. Chem. Phys.* **2011,** *135*, 014707.

57. Xu, T.; Zvelindovsky, A. V.; Sevink, G. J. A.; Lyakhova, K. S.; Jinnai, H.; Russell, T. P., Electric Field Alignment of Asymmetric Diblock Copolymer Thin Films. *Macromolecules* **2005,** *38*, 10788-10798.

58. Xu, T.; Zvelindovsky, A. V.; Sevink, G. J. A.; Gang, O.; Ocko, B.; Zhu, Y.; Gido, S. P.; Russell, T. P., Electric Field Induced Sphere-to-Cylinder Transition in Diblock Copolymer Thin Films. *Macromolecules* **2004,** *37*, 6980-6984.

59. Martin, J. M.; Li, W.; Delaney, K. T.; Fredrickson, G. H., Scft Study of Diblock Copolymer Melts in Electric Fields: Selective Stabilization of Orthorhombic Fddd Network Phase. *Macromolecules* **2018,** *51*, 3369-3378.
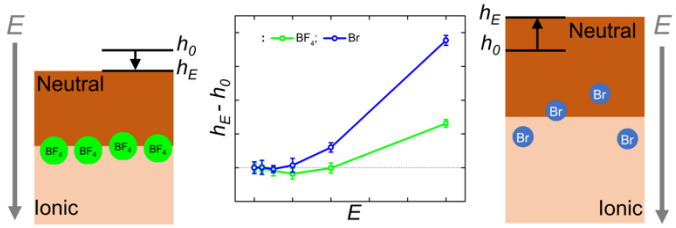
For TOC use only